Evolution of Solar Wind Turbulence from 0.1 to 1 au
during the First Parker Solar Probe – Solar Orbiter Radial Alignment

Daniele Telloni [ID],[1] Luca Sorriso-Valvo [ID],[2,3] Lloyd D. Woodham [ID],[4] Olga Panasenco [ID],[5] Marco Velli [ID],[6]
Francesco Carbone [ID],[7] Gary P. Zank [ID],[8,9] Roberto Bruno [ID],[10] Denise Perrone [ID],[11] Masaru Nakanotani [ID],[8]
Chen Shi [ID],[6] Raffaella D'Amicis [ID],[10] Rossana De Marco [ID],[10] Vamsee K. Jagarlamudi [ID],[10]
Konrad Steinvall [ID],[2] Raffaele Marino [ID],[12] Laxman Adhikari [ID],[8] Lingling Zhao [ID],[8] Haoming Liang [ID],[8]
Anna Tenerani [ID],[13] Ronan Laker [ID],[4] Timothy S. Horbury [ID],[4] Stuart D. Bale [ID],[14,15] Marc Pulupa [ID],[14]
David M. Malaspina [ID],[16,17] Robert J. MacDowall [ID],[18] Keith Goetz [ID],[19] Thierry Dudok de Wit [ID],[20]
Peter R. Harvey [ID],[14] Justin C. Kasper [ID],[21,22] Kelly E. Korreck [ID],[23] Davin Larson [ID],[14] Anthony W. Case [ID],[23]
Michael L. Stevens [ID],[23] Phyllis Whittlesey [ID],[14] Roberto Livi [ID],[14] Christopher J. Owen [ID],[24] Stefano Livi [ID],[25]
Philippe Louarn [ID],[26] Ester Antonucci [ID],[1] Marco Romoli [ID],[27] Helen O'Brien [ID],[4] Vincent Evans [ID],[4] and
Virginia Angelini [ID][4]

[1]National Institute for Astrophysics, Astrophysical Observatory of Torino, Via Osservatorio 20, I-10025 Pino Torinese, Italy
[2]Swedish Institute of Space Physics, Ångström Laboratory, Lägerhyddsvägen 1, SE-751 21 Uppsala, Sweden
[3]National Research Council, Institute for the Science and Technology of Plasmas, Via Amendola 122/D, I-70126 Bari, Italy
[4]Department of Physics, Imperial College London, London SW7 2AZ, UK
[5]Advanced Heliophysics, Pasadena, CA 91106, USA
[6]Earth, Planetary, and Space Sciences, University of California, Los Angeles, CA 90095, USA
[7]National Research Council, Institute of Atmospheric Pollution Research, c/o University of Calabria, I-87036 Rende, Italy
[8]Center for Space Plasma and Aeronomic Research, University of Alabama in Huntsville, Huntsville, AL 35805, USA
[9]Department of Space Science, University of Alabama in Huntsville, Huntsville, AL 35805, USA
[10]National Institute for Astrophysics, Institute for Space Astrophysics and Planetology, Via del Fosso del Cavaliere 100, I-00133 Roma,
Italy
[11]Italian Space Agency, Via del Politecnico snc, I-00133 Roma, Italy
[12]Laboratoire de Mécanique des Fluides et d'Acoustique, Centre National de la Recherche Scientifique, École Centrale de Lyon, Université
Claude Bernard Lyon 1, INSA de Lyon, F-69134 Écully, France
[13]Department of Physics, The University of Texas at Austin, Austin, TX 78712, USA
[14]Space Sciences Laboratory, University of California, Berkeley, CA 94720, USA
[15]Physics Department, University of California, Berkeley, CA 94720, USA
[16]Astrophysical and Planetary Sciences Department, University of Colorado, Boulder, CO 80309, USA
[17]Laboratory for Atmospheric and Space Physics, University of Colorado, Boulder, CO 80303, USA
[18]National Aeronautics and Space Administration, Goddard Space Flight Center, Greenbelt, MD 20771, USA
[19]School of Physics and Astronomy, University of Minnesota, Minneapolis, MN 55455, USA
[20]Laboratoire de Physique et de Chimie de l'Environnement et de l'Espace, Center National de la Recherche Scientifique, 3A Avenue de
la Recherche Scientifique, F-45071 Orléans, France
[21]BWX Technologies, Inc., Washington, DC 20002, USA
[22]Climate and Space Sciences and Engineering, University of Michigan, Ann Arbor, MI 48109, USA
[23]Harvard-Smithsonian Center for Astrophysics, Cambridge, MA 02138, USA
[24]Mullard Space Science Laboratory, University College London, Holmbury St. Mary, RH5 6NT Dorking, UK
[25]Southwest Research Institute, San Antonio, TX 78238, USA
[26]Institut de Recherche en Astrophysique et Planétologie, 9 Avenue du Colonel Roche, F-31028 Toulouse, France
[27]University of Florence, Department of Physics and Astronomy, Via Giovanni Sansone 1, I-50019 Sesto Fiorentino, Italy

ABSTRACT

Corresponding author: Daniele Telloni
daniele.telloni@inaf.it

The first radial alignment between Parker Solar Probe and Solar Orbiter spacecraft is used to investigate the evolution of solar wind turbulence in the inner heliosphere. Assuming ballistic propagation, two 1.5 hr intervals are tentatively identified as providing measurements of the same plasma parcels traveling from 0.1 to 1 au. Using magnetic field measurements from both spacecraft, the properties of turbulence in the two intervals are assessed. Magnetic spectral density, **flatness** and high-order moment scaling laws are calculated. The Hilbert-Huang transform is additionally used to mitigate short sample and poor stationarity effects. Results show that the plasma evolves from a highly Alfvénic, less-developed turbulence state near the Sun, to fully-developed and intermittent turbulence at 1 au. These observations provide strong evidence for the radial evolution of solar wind turbulence.

1. INTRODUCTION

The interplanetary medium is a continuous, highly variable, weakly-collisional plasma outflow from the Sun. In-situ spacecraft observations generally reveal the solar wind far away from the Sun to be in a state of fully-developed turbulence (Coleman 1968; Bruno & Carbone 2013). The energy in electromagnetic and velocity fluctuations, injected at the Sun and during the solar wind expansion into the heliosphere, is channeled towards smaller spatial/time scales through a turbulent cascade until it eventually dissipates. The power spectral density of magnetic and velocity fields within the inertial range shows a power-law dependence similar to that observed in fluid turbulence (Kolmogorov 1941; Tu & Marsch 1995). In the fast solar wind, a low-frequency spectral break, which separates the inertial range from (larger) injection scales, moves to larger and larger scales with distance from the Sun (Bruno & Carbone 2013). At scales below the inertial range, ions become unmagnetized and plasma dynamics is governed by particle kinetic properties. There, another spectral break is observed, whose frequency also depends on radial distance from the Sun, consistently with proton cyclotron resonance conditions (Bruno & Trenchi 2014). In addition to spectral breaks, other properties of turbulence (such as Alfvénic content, intermittency, anisotropy) also evolve with heliocentric distance (see the review by Bruno & Carbone 2013, and references therein).

One way to study the radial evolution of solar wind turbulence properties is to consider plasma coming from the same solar source. A well-defined high-speed stream observed by Helios at different heliodistances during three consecutive solar rotations was used to study the radial evolution of turbulence (Bavassano et al. 1981, 1982a,b; He et al. 2013) and intermittency (Bruno et al. 2003, 2014a) in the inner heliosphere. More recently, by means of reprocessed particle data from the Helios mission, 16 intervals of unperturbed high-speed plasma, from three different coronal holes and at different radial distances between 0.3 and 1 au, have been identified to investigate the large-scale physics and thermodynamics of the solar wind (Perrone et al. 2019a,b).

An ideal (although rarely used) approach is to follow the same plasma parcel during its expansion. This method requires two or more radially-aligned spacecraft at different distances. The first instance of these exceptional cases occurred when the Helios 1 and Helios 2 sampled the same high-speed stream plasma at ~ 0.51 and ~ 0.72 au, respectively (Schwartz & Marsch 1983). The authors found clear evidence that particle adiabatic invariants are not conserved, suggesting some ion perpendicular heating. Successive alignments in the inner heliosphere, between Wind and MESSENGER (Bruno & Trenchi 2014; Bruno et al. 2014b; Telloni et al. 2015), and in the outer heliosphere, between Wind and Ulysses (Bruno & Trenchi 2014) or ACE and Ulysses (D'Amicis et al. 2010), were used to study the evolution of the solar wind turbulence between ~ 0.4 and ~ 5.3 au systematically. These studies showed that the ion spectral break moves to higher and higher frequencies approaching the Sun (D'Amicis et al. 2010; Bruno & Trenchi 2014). In addition, Bruno et al. (2014b) found that the spectral slope of the dissipative range depends strongly on the power associated with the fluctuations within the inertial range, i.e. the higher the power, the steeper the slope. Finally, the high-frequency magnetic fluctuations beyond the spectral break show a character compatible with left-handed ion cyclotron waves and right-handed kinetic Alfvén waves, with the low-frequency limit of these fluctuations following the radial evolution of the ion spectral break (Telloni et al. 2015).

Thanks to the new inner heliospheric missions Parker Solar Probe (PSP, Fox et al. 2016), launched in August 2018, and Solar Orbiter (SolO, Müller et al. 2020), launched in February 2020, a new golden era for solar wind physics is upon us. PSP is observing a completely unexplored environment close to the Sun, while SolO will combine both high-resolution in-situ measurements and remote-sensing observations (Zouganelis et al. 2020) aiming to accurately

determine magnetic connectivity between the solar wind plasma and its source regions at the Sun. Indeed, the synergy between the two spacecraft allows for a detailed mapping of the inner heliosphere (Velli et al. 2020). In particular, radial alignments between the two probes allow the study of the evolution of the solar wind at distances never reached before. The first line-up between PSP and SolO occurred in September 2020, when PSP (approaching perihelion during its 6th solar encounter) and SolO were orbiting at ~ 0.1 and ~ 1 au, respectively.

The aim of the present Letter is to exploit this PSP – Solo radial alignment to study, for the first time, the radial evolution of the solar wind turbulence properties, namely magnetic spectra, compressibility and intermittency, from near the Alfvén radius (Goelzer et al. 2014) out to Earth orbit.

2. PSP – SOLO RADIAL ALIGNMENT IDENTIFICATION

The identification of the time intervals corresponding to the same plasma parcel observed at PSP and SolO distances during their radial alignment with the Sun is based on the ballistic approach sketched in the cartoon of Fig. 1 (top panel). The condition for radial alignment requires that the longitude at PSP, $\Phi_{\rm PSP}$, at the instant t_0 when the spacecraft samples the plasma parcel is equal to that at SolO, $\Phi_{\rm SolO}$, at the instant $t_0 + \Delta t$, where Δt is the plasma transit time from PSP to SolO, i.e.

$$
\begin{aligned}
\Phi_{\rm PSP}(t_0) &= \Phi_{\rm SolO}[t_0 + \Delta t] \\
&= \Phi_{\rm SolO}[t_0 + \Delta R/V_{\rm PSP}(t_0)] \\
&= \Phi_{\rm SolO}[t_0 + (R_{\rm SolO}(t_0 + \Delta t) - R_{\rm PSP}(t_0))/V_{\rm PSP}(t_0)],
\end{aligned}
\tag{1}
$$

where ΔR is the radial separation between PSP and SolO, located at $R_{\rm PSP}$ and $R_{\rm SolO}$, respectively, and $V_{\rm PSP}$ is the solar wind speed observed at PSP.

On the basis of the PSP and SolO ephemerides and the plasma speed observed at PSP (in the inertial Radial Tangential Normal (RTN) frame) by the SPAN-Ai top-hat electrostatic analyzer (part of the SWEAP suite onboard PSP, Kasper et al. 2016), it follows that the plasma crossing PSP on 2020/09/27 (at $\simeq 04:00$ UT) could be sampled by SolO on 2020/10/02 (around $\simeq 00:00$ UT). Applying a tolerance of $\pm 1.5°$ longitude for the radial alignment, time intervals of 1.5 hours centered on the above times are thus identified as corresponding to the same plasma parcels.

From Eq. 1 one sees that the timings relative to the radial alignment depend on $V_{\rm PSP}$ and possible subsequent acceleration, especially for SolO. The extension of the magnetic parcel under study is so short (hours) with respect to the much longer transit time (days) that uncertainties related to plasma velocity measurements (e.g. moments of ion distribution functions include the contribution from the proton beam, which can be very large at times) as well as velocity field fluctuations (from turbulence and/or switchbacks) may easily lead to misalignments. In order to address this issue and check the goodness of the selected time intervals, a complementary strategy has been adopted. The plasma speed at PSP is assumed to range from 250 to 350 km s^{-1} in steps of 1 km s^{-1}. From $N = 100$ different propagation speeds, N different pairs of 1.5 hr time intervals at PSP and SolO, relative to each potential radial alignment, are thus identified. The pair of time intervals for which the cross-correlation between the magnetic field magnitude $|\mathbf{B}|$ measured at PSP (by the fluxgate magnetometer of the FIELDS suite, Bale et al. 2016) and SolO (by the MAG magnetometer, Horbury et al. 2020) maximizes is assumed to be the one corresponding to the same solar wind plasma observed at 0.1 and 1 au. The magnetic field magnitude in the same plasma parcel may indeed be expected to be relatively well correlated when observed at different distances, since in-situ driving of turbulence may balance dissipation (the reader is e.g. referred to Zank et al. 2017, for the relevant theory). The time intervals with the highest correlation in $|\mathbf{B}|$ (0.72 at 0-lag) are found to be 2020/09/27 03:15 – 04:45 UT at PSP and 2020/10/01 21:34 – 23:04 UT at SolO, corresponding to a solar wind bulk speed of 320 km s^{-1} at PSP. Both the temporal localization of the parcel and the wind speed at PSP are in good agreement with the independent estimate based on the measured speed at PSP (315 km s^{-1}), showing the robustness of the correlation analysis.

The bottom panels of Fig. 1 show side (left panel) and top (right panel) views of the ecliptic plane during the PSP – Solo line-up, when the two spacecraft had a radial separation of 0.9 au, with PSP approaching perihelion close to 0.1 au, i.e. 20 R$_\odot$, and SolO orbiting at a radial distance of about 1 au.

Unfortunately, during the radial alignment, plasma measurements from SolO were unavailable, thus preventing checks of the solar wind speed at SolO. In order to address this shortcoming, the DSCOVR speed data were time-shifted by about +9.3 days (which accounts for the solar rotation and the different longitude of SolO and DSCOVR). Despite the approximate approach, the resulting expected speed at SolO during the radial alignment is about 324 km s^{-1},
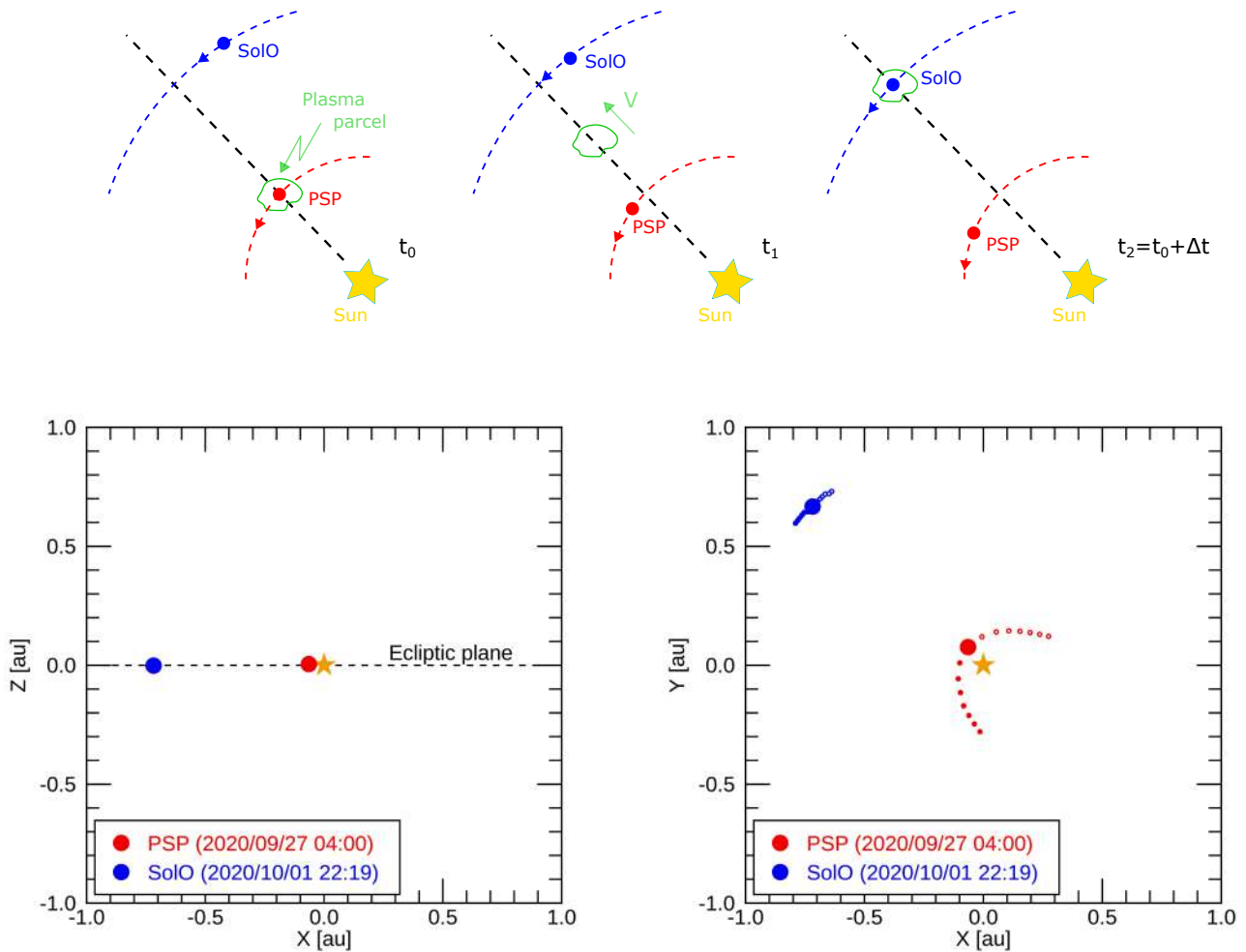
Figure 1. Top panel: cartoon of the encounters of the same plasma parcel with PSP and SolO during their radial alignment. Bottom panels: positions of PSP (red) and SolO (blue) relative to the Sun (yellow star), in the XZ (left) and XY (right) planes of the heliocentric ecliptic coordinate frame, at the times of the crossing of the same solar wind plasma. The positions the probes had in the seven days before and after the radial alignment are also shown, as empty and full points of smaller size, respectively.

only a slight increase with respect to that observed at PSP, confirming the quality of the PSP – SolO radial alignment identification.

Finally, in order to check whether the plasma observed by PSP and SolO in the selected intervals comes from the same source region at the Sun (further corroborating the above findings) the coronal origins of the solar wind observed by PSP on 2020/09/27 and by SolO on 2020/10/02 have been assessed. Spacecraft positions have been projected onto the source surface and then down to the height of 1.16 $R_{\odot}$, using a Potential Field Source Surface (PFSS) model (Schrijver & De Rosa 2003), as displayed in Fig. 2. The source surface height has been adjusted to 2.0 $R_{\odot}$, following the magnetic field polarity changes observed by SolO on 2020/09/27 (left panel of Fig. 2). A detailed description of the solar wind source mapping can be found in Panasenco et al. (2020). As follows from the comparison between the panels of Fig. 2, during the time periods corresponding to the radial alignment, PSP (left panel, in blue) and SolO (right panel, in orange) were connected to the same equatorial extension of the southern polar coronal hole at $240 - 250°$ Carrington Longitude. On 2020/09/27 PSP, at perihelion, was fast sampling this area, while SolO took a little longer to pass through it due to the natural expansion of the wind and its slower motion. The fact that SolO

is magnetically connected to the same region at the Sun as PSP confirms that they sample the same plasma parcel, embedded in an Alfvénic low-speed stream coming from the same South coronal hole extension.
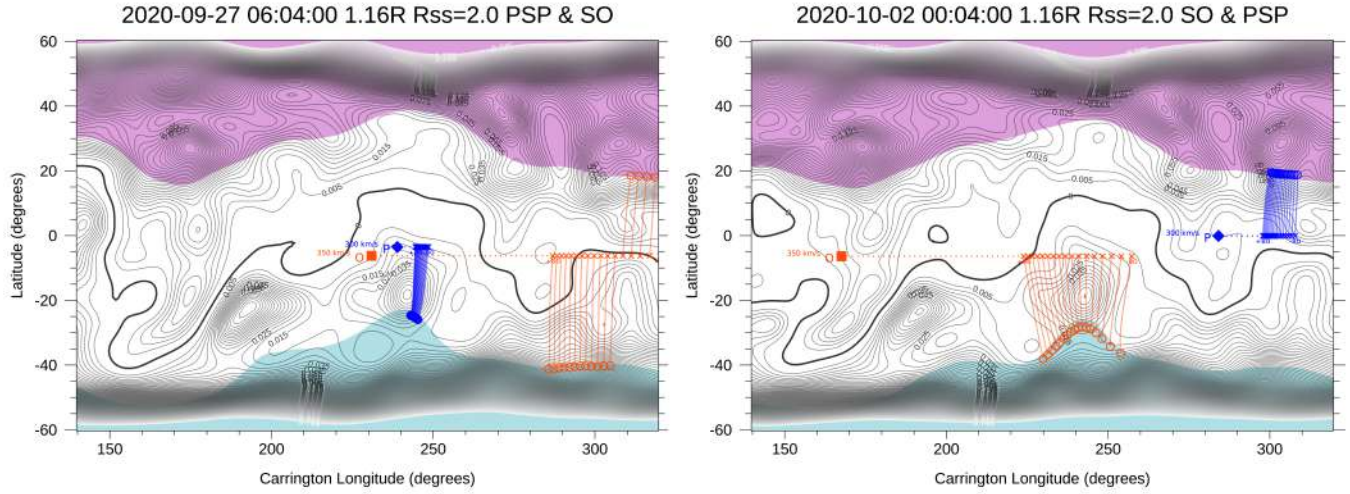
Figure 2. Potential Field Source Surface (PFSS) $|\mathbf{B}|^2$ contour maps and solar wind magnetic foot-points along the PSP and SolO trajectories for the selected time intervals. The projections of PSP (blue diamonds) and SolO (orange squares) locations on the source surface (blue and orange crosses) and down to the solar wind source region (blue and orange circles), calculated for the height of 1.16 $R_\odot$ and based on in-situ solar wind speed measurements ± 80 km s^{-1}, are displayed. Open magnetic field regions are shown in blue (negative magnetic polarity) and violet (positive magnetic polarity), and the neutral line is in thick black.

3. EVOLUTION OF TURBULENCE FROM PSP TO SOLO

The magnetic field magnitude and components in the heliographic RTN coordinate system, along with the angle between the magnetic field vector and the radial direction $\theta_{RB} = \arccos(B_R/|\mathbf{B}|)$, relative to the time periods selected in § 2 at PSP and SolO, are displayed in the three top panels of Figs. 3 and 4, respectively, which overall span a time interval of 1 day. Specifically, PSP/FIELDS ~ 292 Hz and SolO/MAG 64 Hz burst-mode magnetic field data have been used. As expected, because they measure the same plasma parcel, the PSP and SolO periods share common characteristics. Specifically, during both intervals, $|\mathbf{B}|$ is quite smooth (revealing that the fluctuations in the wind are largely incompressible) and slightly increasing, the magnetic polarity is negative ($B_R < 0$), and the magnetic field is fairly radial ($\theta_{RB} \sim 180°$). The observed solar wind plasma hence belongs to a quiescent region, namely a region with exceptionally smooth magnetic field (free of switchbacks) and Parker-spiral-like direction of the magnetic field (Dudok de Wit et al. 2020; Malaspina et al. 2020).

In order to assess the characteristics of turbulence in the plasma parcel observed at two different evolution stages, standard diagnostics for spectral power, compressibility, and intermittency of the magnetic field fluctuations have been used.

The top-left panel of Fig. 5 shows the spectrum of the magnetic field vector fluctuations $\delta\mathbf{B}^2$. Power-law fits have been performed at typical fluid scales, between 3×10^{-3} and 10^{-1} Hz in the spacecraft frame, which can be identified as the inertial range of turbulence. The fitted spectral exponents are indicated in the legend. As expected, PSP data shows much larger power, due to the larger amplitude of fluctuations at 0.1 au. SolO interval displays a power-law spectrum with scaling exponent α compatible with the standard Kolmogorov fully-developed turbulence, $\alpha \sim 5/3$ (Kolmogorov 1941). On the contrary, PSP shows a shallower spectrum ($\alpha \sim 3/2$, Chen et al. 2020; Duan et al. 2020), suggesting a less-developed, more Alfvénic turbulence (Bruno & Carbone 2013), as observed during quiescent intervals (Dudok de Wit et al. 2020; Malaspina et al. 2020). Some caveats are necessary in interpreting the PSP results since the flow and magnetic fields in the interval of interest are highly aligned (bottom panel of Fig. 3), the implication being that advected quasi-2D structures are essentially invisible (Zank et al. 2020) and hence their contribution is difficult to assess. **It is worth noting that the power spectrum at SolO exhibits a high-frequency break**
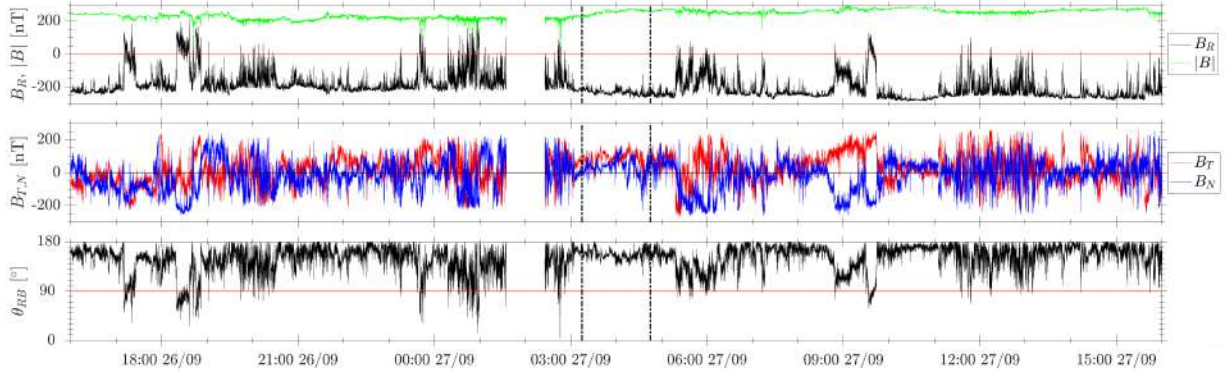
Figure 3. Magnetic field data at PSP in the 1-day interval centered on 2020/09/27 03:15 – 04:45 (delimited by vertical dashed lines). From top to bottom: B_R and $|\mathbf{B}|$, B_T and B_N, and angle θ_{RB} between the radial direction and $\mathbf{B}$.
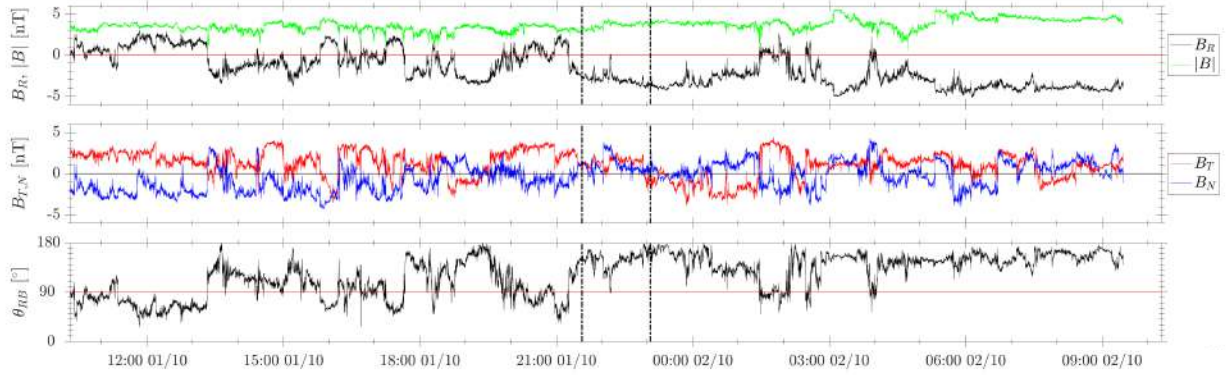

Figure 4. Same as Fig. 3, but for 1-day SolO observations centered on the time periods 2020/10/01 21:34 – 23:04.

around 0.2 Hz, which marks the transition from fluid to kinetic scales. According to previous findings (e.g. Bruno & Trenchi 2014; Telloni et al. 2019a), this break is close to the proton gyro-frequency, thus suggesting the likely role played by the ion-cyclotron resonance mechanism in the spectral cascade.

The highly Alfvénic nature of PSP data was confirmed by the smaller compressibility factor $C = \delta|\mathbf{B}|^2/\delta\mathbf{B}^2$ (i.e. the ratio between the spectra of the magnetic field magnitude and vector fluctuations, Bavassano et al. 1982b), shown in the top-right panel of Fig. 5 and used here as a proxy of Alfvénicity[1]. **Indeed, bearing in mind that the solar wind consists mainly of a mixture of propagating non-compressive Alfvénic fluctuations and compressive magnetic structures advected by the wind, a low magnetic compressibility clearly indicates a dominance of Alfvénic over compressive fluctuations and, in turn, a high Alfvénic content of the solar wind.** The turbulent fluctuations observed by SolO are less Alfvénic, in agreement with the known general behavior of the Alfvénicity of tending to decay with increasing distance from the Sun. Such decay could result from nonlinear interactions (Bruno & Carbone 2013; Zank et al. 2020), transversal velocity and magnetic field shears generated by the solar wind expansion (Shi et al. 2021), or other mechanisms such as parametric decay (e.g. Malara & Velli 1996; Bruno et al. 2014a). On the other hand, the higher Alfvénicity at PSP may result in stronger decorrelation between

---

[1] The Alfvénic character of the fluctuations at PSP is also clearly revealed by the high degree of correlation between magnetic and velocity field fluctuations, i.e. high values of cross-helicity, and by the rather good equipartition between magnetic and kinetic energies, i.e. low values of residual energy (not shown).
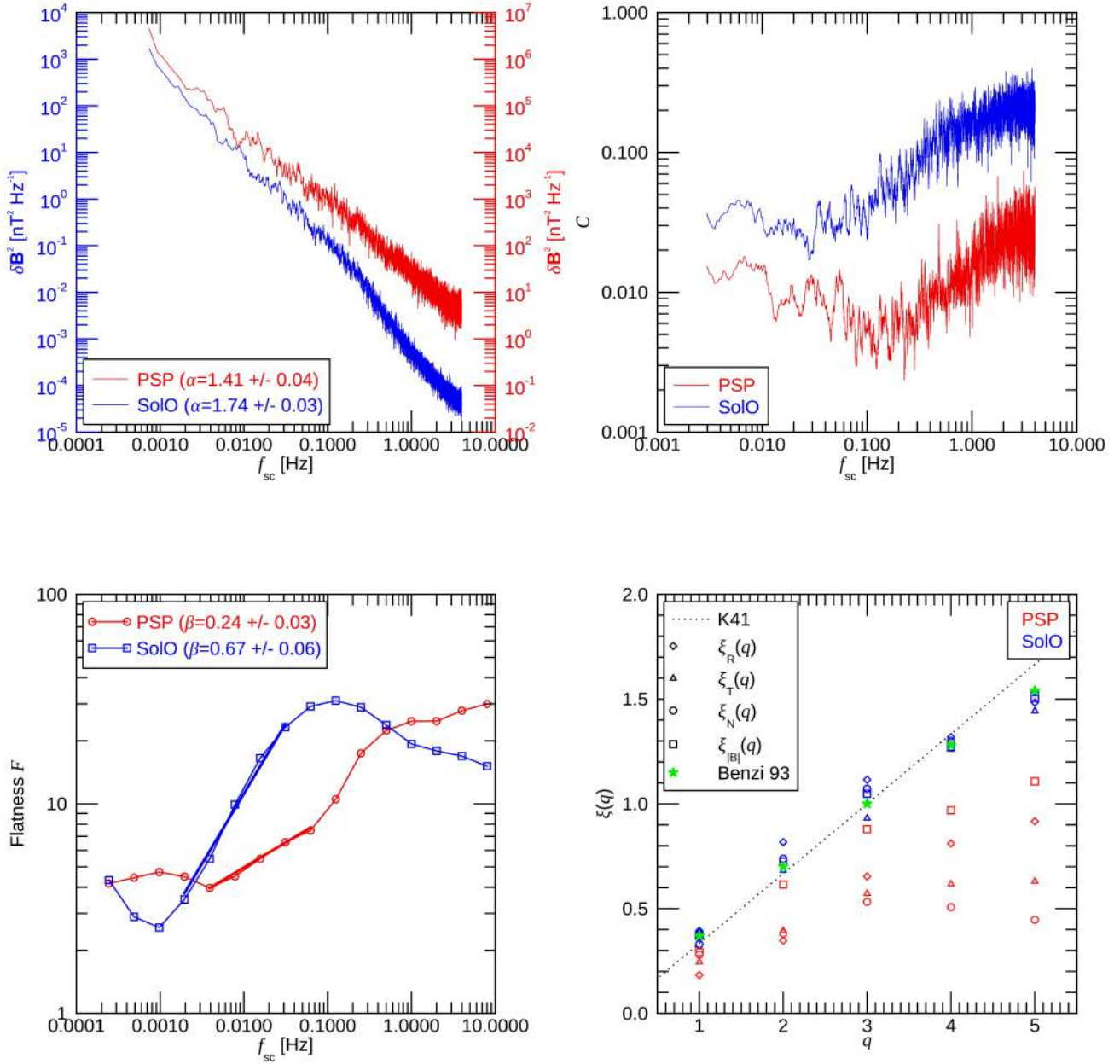
Figure 5. Trace of the magnetic spectral matrix $\delta\mathbf{B}^2$ (top-left), magnetic compressibility spectrum C (top-right), **flatness** $\mathcal{F}$ as a function of the spacecraft frequency (bottom-left), for PSP (red) and SolO (blue) radially aligned intervals. **Power-law fits are displayed as thick lines, while** relative scaling exponents are reported in the legends. Bottom-right: comparison of the scaling exponents ξ_q of the qth-order structure functions for PSP (red) and SolO (blue) magnetic field RTN components and magnitude (represented by different symbols as reported in the legend). As a comparison, exponents for velocity fluctuations in the inertial range of hydrodynamic turbulence (**green** stars, Benzi et al. 1993) and the classical K41 ($q/3$) Kolmogorov law (dotted line, Kolmogorov 1941) are also displayed.

the interacting magnetic turbulent structures, reducing the efficiency of the nonlinear cascade (Dobrowolny et al. 1980; Smith et al. 2009; Marino et al. 2011) and leading to a shallower power spectrum.

The presence of intermittency (a characteristic feature of non-linear turbulence, Anselmet et al. 1984; Frisch 1995; Bruno & Carbone 2013) was evaluated through the ratio between the fourth and the squared second-order structure functions, i.e. the **flatness $\mathcal{F}(1/f) = \langle\Delta\mathbf{B}^4\rangle/\langle\Delta\mathbf{B}^2\rangle^2$, where $\Delta\mathbf{B}(t, 1/f)$ are increments of the magnetic field vector across a timescale $1/f$ (f is the frequency). The flatness is** typically used to describe deviation from Gaussian-distributed fluctuations (e.g. Frisch 1995; Dudok de Wit et al. 2013; Zhao et al. 2020), **for which $\mathcal{F} = 3$.** This quantity is shown in the bottom-left panel of Fig. 5. Both intervals show a power-law scaling $\mathcal{F} \sim f^\beta$ in the inertial range (**approximately** from $\sim 3 \times 10^{-3}$ to $\sim 5 \times 10^{-2}$ Hz), **as indicated by the thick solid lines in the figure. As a reference, in fluid turbulence $\beta \sim 0.1$ (Frisch 1995), while in space plasmas values between 0.2 and 0.5 have been observed (Sorriso-Valvo et al. 2019; Quijia et al. 2021).** The **flatness** increases **slowly at PSP ($\beta = 0.24 \pm 0.03$), indicating poorly developed intermittency, and** more rapidly at SolO, **where the large exponent ($\beta = 0.67 \pm 0.06$) suggests an extremely** efficient energy cascade (**Carbone & Sorriso-Valvo 2014**). This could be also related to the decrease of the Alfvénic content with distance, allowing the coherent structures advected by the wind to emerge more clearly and control the high-order statistics (Zank et al. 2020).

To ensure statistical significance and ergodicity, the same quantities were also estimated in extended intervals of 2.17 hr for PSP (2020/09/27 03:05 – 05:15) and 4 hr for SolO (2020/10/01 21:20 – 2020/10/02 01:20). It is worth noting that the extended intervals also originated at the same solar source (though not strictly corresponding to the same plasma parcel), and the in-situ magnetic field characteristics remained approximately stationary. Such a choice also accounts for a ± 5 km s^{-1} uncertainty in the wind bulk speed used for the identification of the plasma parcel (see § 2). The results obtained in the extended intervals fully confirmed those obtained using the shorter intervals.

Finally, in order to mitigate possible effects of non-stationarity and large-scale structures, intermittency was also assessed using the Hilbert-Huang technique (see e.g. Huang et al. 1998, 2008; Carbone et al. 2018; Telloni et al. 2019b) to obtain the scaling exponents ξ_q of the qth-order structure functions. These were estimated for the magnetic field components and magnitude by resampling and bootstrapping the least-squares fit in the inertial range of the generalized Hilbert spectra, up to the fifth order (Carbone et al. 2020). As shown in the bottom-right panel of Fig. 5, the deviation from linear order dependence typical of intermittent turbulent flows is observed at SolO for all the magnetic field components and magnitude. Values from a standard experiment of fluid turbulence (Benzi et al. 1993) are shown for comparison. On the other hand, at PSP the scaling exponents **are too small, in some cases decreasing with order, and in general** do not compare with standard turbulence (an identified property of the quiescent regions Dudok de Wit et al. 2020), suggesting once more the poorly-developed nature of the turbulent cascade or the presence of **strong** superposed Alfvénic fluctuations. The second-order scaling exponent $\xi(2) \equiv \alpha - 1$ confirms the spectral observation that the magnetic power has a Kolmogorov scaling for SolO, but shallower scaling for PSP. Similarly, the Hurst number $\mathcal{H} = \xi(1)$ (Flandrin et al. 2004; Carbone et al. 2018), a measure of the memory in the time series (Wang et al. 2000), is much smaller in the PSP interval (mean and standard deviation for the three components being $\mathcal{H} \sim 0.23 \pm 0.05$) than for SolO ($\mathcal{H} = 0.37 \pm 0.04$), indicating that the magnetic field at 0.1 au does not show strong memory, which would be expected of intermittent turbulent fluctuations.

The statistical analysis of the intervals at PSP and SolO suggests that the turbulence is evolving during the expansion. Power spectra, intermittency and compressibility indicate that the nonlinear interactions between Alfvén waves may not yet have had time to fully develop at 0.1 au, where the solar wind sampled by PSP is still pristine and unaffected by stream-stream interactions. On the contrary, the same plasma has considerably evolved at 1 au, where the Alfvénic fluctuations have become smaller. At SolO, the nonlinear interactions might have efficiently formed a fully-developed spectrum, additionally building up small-scale intermittent structures and long-term memory. Alternatively, the decrease of the Alfvénic fluctuations could have exposed the intermittent nature of the advected coherent structures.

ACKNOWLEDGMENTS

REFERENCES

Anselmet, F., Gagne, Y., Hopfinger, E. J., et al. 1984, JFM, 140, 63

Bale, S. D., Goetz, K., Harvey, P. R., et al. 2016, SSRv, 204, 49

Bavassano, B., Dobrowolny, M., Mariani, F., & Ness, N. F. 1981, JGRA, 86, 1271

Bavassano, B., Dobrowolny, M., Mariani, F., & Ness, N. F. 1982, JGRA, 87, 3617

Bavassano, B., Dobrowolny, M., Fanfoni, G., Mariani, F., & Ness, N. F. 1982, SoPh, 78, 373

Benzi, R., Ciliberto, S., Tripiccione, R., et al. 1993, PhRvE, 48, R29

Bruno, R., Carbone, V., Sorrivo-Valvo, L., & Bavassano, B. 2003, JGRA, 108, 1130

Bruno, R., & Carbone, V. 2013, LRSP, 10, 2

Bruno, R., & Trenchi, L. 2014, ApJL, 787, L24

Bruno, R., Telloni, D., Primavera, L., et al. 2014, ApJ, 786, 53

Bruno, R., Trenchi, L., & Telloni, D. 2014, ApJL, 793, L15

Carbone, F., & Sorriso-Valvo, L. 2014, EPJE, 37, 61

Carbone, F., Sorriso-Valvo, L., Alberti, T., et al. 2018, ApJ, 859, 27

Carbone, F., Telloni, D., Sorriso-Valvo, L., et al. 2020, Univ, 6, 116

Chen, C. H. K., Bale, S. D., Bonnell, J. W., et al. 2020, ApJS, 246, 53

Coleman, P. J. Jr 1968, ApJ, 153, 371

D'Amicis, R., Bruno, R., Pallocchia, G., et al. 2010, ApJ, 717, 474

Dobrowolny, M., Mangeney, A., & Veltri, P. 1980, PhRvL, 45, 144

Duan, D., Bowen, T. A., Chen, C. H. K., et al. 2020, ApJS, 246, 55

Dudok de Wit, T., Alexandrova, O., Furno, I, Sorriso-Valvo, L., & Zimbardo, G. 2013, Ssrv, 178, 665

Dudok de Wit, T., Krasnoselskikh, V. V., Bale, S. D., et al. 2020 ApJS, 246, 39

Flandrin, P., Rilling, G., & Goncalves, P. 2004, ISPL, 11, 112

Fox, N. J., Velli, M., Bale, S. D., et al. 2016, SSRv, 204, 7

Frisch, U. 1995, Turbulence (Cambridge: Cambridge Univ. Press)

Goelzer, M. L., Schwadron, N. A., & Smith, C. W. 2014, JGRA, 119, 115

He, J., Tu, C., Marsch, E., Bourouaine, S., & Pei, Z. 2013, ApJ, 773, 72

Horbury, T. S., O'Brien, H., Carrasco Blazquez, I., et al. 2020, A&A, 642, A9

Huang, N. E., Shen, Z., Long, S. R., et al. 1998, RSPSA, 454, 903

Huang, Y. X., Schmitt, F. G., Lu, Z. M., & Liu, Y. L. 2008, EL, 84 40010

Kasper, J. C., Abiad, R., Austin, G., et al. 2016, SSRv, 204, 131

Kolmogorov, A. 1941, DoSSR, 30, 301

Malara, F., & Velli, M. 1996 PhPl, 3, 4427

Malaspina, D. M., Halekas, J., Berčič, L., et al. 2020, ApJS, 246, 21

Marino, R., Sorriso-Valvo, L., Carbone, V., et al. 2011, P&SS, 59, 592

Müller, D., St. Cyr, O. C., Zouganelis, I., et al. 2020, A&A, 642, A1

Panasenco, O., Velli, M., D'Amicis, R., et al. 2020, ApJS, 246

Perrone, D., Stansby, D., Horbury, T. S., & Matteini, L. 2019, MNRAS, 483, 3730

Perrone, D., Stansby, D., Horbury, T. S., & Matteini, L. 2019, MNRAS, 488, 2380

Quijia, P., Fraternale, F., Stawarz, J. E., et al. 2021, MNRAS, 503, 4815

Schrijver, C. J., & De Rosa, M. L. 2003, SoPh, 212, 165

Schwartz, S. J., & Marsch, E. 1983, JGRA, 88, 9919

Shi, C., Velli, M., Panasenco, O., et al. 2021, A&A, in press

Smith, C. W., Stawarz, J. E., Vasquez, B. J., Forman, M. A., & MacBride, B. T. 2009, PhRvL, 103, 201101

Sorriso-Valvo, L., De Vita, G., Fraternale, F., et al. 2019, FrP, 7, 108

Telloni, D., Bruno, R., & Trenchi, L. 2015, ApJ, 805, 46

Telloni, D., Carbone, F., Bruno, R., et al. 2019, ApJL, 885, L5

Telloni, D., Carbone, F., Bruno, R., et al. 2019, ApJ, 887, 160

Tu, C.-Y., & Marsch, E. 1995, SSRv, 73, 1

Velli, M., Harra, L. K., Vourlidas, A., et al. 2020, A&A, 642, A4

Wang, G., Antar, G., & Devynck, P. 2000, PhPl, 7, 1181

Zank, G. P., Adhikari, L., Hunana, P., et al. 2017, ApJ 835, 147

Zank, G. P., Nakanotani, M., Zhao, L.-L., Adhikari, L., & Telloni, D. 2020, ApJ, 900, 115

Zhao, L.-L., Zank, G. P., Adhikari, L., et al. 2020, ApJ, 898, 113

Zouganelis, I., De Groof, A., Walsh, A. P., et al. 2020, A&A, 642, A3